2015-03-01

Temperature and Stress Effect Modeling in Fatigue of H13 Tool Steel at Elevated Temperatures with Applications in Friction Stir Welding

Bradley Valiant Jones
Brigham Young University - Provo

Temperature and Stress Effect Modeling in Fatigue of H13 Tool Steel at Elevated Temperatures with Applications in Friction Stir Welding

Bradley Valiant Jones

A thesis submitted to the faculty of
Brigham Young University
in partial fulfillment of the requirements for the degree of

Master of Science

Carl D. Sorensen, Chair
Tracy W. Nelson
C. Shane Reese

Department of Mechanical Engineering

Brigham Young University

March 2015

ABSTRACT

Temperature and Stress Effect Modeling in Fatigue of H13 Tool Steel at Elevated Temperatures with Applications in Friction Stir Welding

Bradley Valiant Jones
Department of Mechanical Engineering, BYU
Master of Science

Tooling reliability is critical to welding success in friction stir welding, but tooling fatigue is not well understood because it occurs in conditions that are often unique to friction stir welding. A fatigue study was conducted on a commonly used tooling material, H13 tool steel, using constant stress loading at temperatures between 300°C and 600°C, and the results are presented. A model is proposed accounting for temperature and stress effects on fatigue life, utilizing a two-region Arrhenius temperature model. A transition in temperature effect on fatigue life is identified. Implications of the temperature effect for friction stir welding suggest that tooling fatigue life dramatically decreases above 500°C and accelerated testing should be conducted below 500°C.

Keywords: friction stir welding, H13 tool steel, Arrhenius model, elevated temperature fatigue, reliability, accelerated testing

ACKNOWLEDGMENTS

I am grateful for all the people that supported me and helped me through this process, especially my family. Without the support and love of my wife, Kayla, I would not have been able to complete this research. I am also indebted to Dr. Carl Sorensen for his continual guidance, encouragement, and wisdom that helped me achieve more than I thought I was capable of achieving. Lastly, I owe a special thanks to Denis Delagnes for sending me his doctoral dissertation, which was invaluable in conducting this research.

TABLE OF CONTENTS

LIST OF FIGURES

LIST OF TABLES

1 INTRODUCTION

In friction stir welding, a high strength tool is plunged into the metal plates that are to be welded, and under high torques the rotating tool uses friction to heat the plates sufficiently to soften them, without melting the plates. The rotating tool then traverses the length of the seam, blending the softened metal from the adjoining plates and thus forming a weld. The welding tool geometry and materials are selected to withstand the extreme forces and temperatures inherent in such a process. For the welding of steel, tools are commonly constructed of cermets, such as tungsten carbide or pCBN (Rai, De, Bhadeshia, & DebRoy 2011). For the welding of aluminum, steel tools are commonly used, since they are of a sufficient strength and are significantly more affordable (Rai et al. 2011).

Tool reliability is important to weld quality, since tool failure can damage the weld. In an effort to improve tool life there have been several studies conducted, most either studying the effect of tool geometry on tool life (Prado 2003; Rai et al. 2011) or the effect of tool material (Rai et al. 2011). Concurrent with these studies, it has been observed that tool life is affected by welding parameters, but there have been no studies that have sought to quantify the effects of welding conditions (specifically temperature) on tool life (not true in general). Prado *et al.* suggested that another important factor that influences tool life is process parameters (Prado 2003), particularly welding speed, though their study did not investigate this factor in depth.

None of these studies go as far as attempting to predict probability of tool failure (a reliability model), instead simply demonstrating that tool life is improved with a change in geometry or material.

Just as there are currently no reliability models for friction stir welding tools, there likewise have been no studies on the effects of welding temperature on tool life. One reason for this is that under traditional weld speed and rotational speed control, weld temperature is free to drift during welding. The development of temperature-controlled welding methodologies, though, has brought the temperature effect into focus as a worthwhile point of study. This is of particular importance since in tool life studies of welding speed and rotational speed effects, these effects have always been confounded with the unknown temperature effect.

This study has sought to enable accelerated testing of friction stir welding tooling by identifying a regime in which accelerated testing could be performed. Though this thesis has not attempted to fill all of the identified opportunities, it has laid important groundwork by making the following contributions:

1. A fatigue life distribution has been proposed for rotating bending fatigue of H13 at elevated temperatures.
2. Temperature and stress acceleration of fatigue life has been modeled in the high cycle fatigue (HCF) regime for H13.
3. A significant transition in fatigue behavior with temperature has been identified for H13 near 537°C, indicating a change in failure mode.

2 BACKGROUND

2.1 Fatigue of FSW tooling

Though studies on tool wear have made the most significant contribution to understanding the effects of welding parameters (Fernandez & Murr 2004; Prado 2003), other failure modes have been observed in research. In a study conducted by Nielsen (referenced in Arora *et al.*), an H13 tool had its pin shear off during welding of Al 7075. Arora *et al.* attributed this failure to operation conditions that had the tool stressed nearly to its maximum shear strength, but Arora's study did not seek to establish the mode of failure nor the life of the tool under these conditions (Arora, Mehta, De, & DebRoy 2012). Similarly, Andrews found that a tool (of unspecified material composition) lasted over 1 km in welding of 6XXX series aluminums, but failed after only 2 m in welding 7XXX series aluminums (Andrews 2013). While welding with an MP159 alloy tool in 16 mm 7075 plate, Colegrove & Shercliff also ran into tool breakage (2003). All of these observed failures clearly suggest a potential fatigue failure mechanism. The most significant study was performed at Hitachi, in which tool life was calculated based on regular use conditions to be around 10^6 cycles. An accelerated stress test was then conducted, resulting in failures around 10^3 cycles. Takai *et al.* indicated that the data was found to compare favorably with data for rotating bending fatigue of the tool material at room temperature. Unfortunately, without any of the actual data or the life-estimating reliability model being given, and not knowing what tool material was used, the results of this study cannot be

explored further. Fortunately, the study has demonstrated that friction stir welding tools are susceptible to fatigue and that fatigue modeling can accurately predict tool life (Takai, Ezumi, Aota, & Matsunaga 2007). Before understanding the effect of welding parameters on fatigue life, it is necessary to understand fatigue behavior of the base tool material outside of the context of friction stir welding. For this study, the chosen material was AISI H13 hot work tool steel. H13 was chosen because is commonly used for FSW tools in the welding of aluminum alloys (Rai et al. 2011).

2.2 Literature on fatigue of H13

H13 is part of a family of 5% chromium hot-work tool steels, of which H11 and H13 are the most commonly used. H13 has a slightly higher vanadium content than H11 and thus is more wear resistant, but this is traded for lower fracture toughness (Philip 1990). There is a large body of literature on fatigue of H13 tool steel and because a common industrial use of H13 is in forging dies, most of the studies on fatigue of H13 have sought to model those operating conditions. As a result, studies on fatigue of H13, as well as the very similar H11 tool steel, mostly focus on high strain isothermal cycling or thermomechanical cycling, thus leading to low cycle fatigue (failure in less than 10^4 cycles) (Engberg & Larsson 1988; Velay 2005). Such conditions, however, do not correspond to typical operating conditions for friction stir welding. A study by Arora *et al.* found that the stresses in tools during the welding of AA6061 were below the yield strength of H13, which would correspond to the high-cycle fatigue regime (Arora et al. 2012). DebRoy, De, Bhadeshia, Manvatkar, & Arora specify that bending stresses in tools can be as high 1500 MPa (2012) which is slightly above the ultimate strength of H13 at room temperature (Philip 1990). Such a range of stresses clearly suggests that tool failures can

occur due to both high cycle fatigue and low cycle fatigue (LCF) when bending stresses approach these high levels.

Despite the operational differences for the use of hot-work tool steels between forging dies and friction stir welding, there are a number of important properties of H13 demonstrated by these studies of low cycle fatigue. Velay *et al.* (2005) collected extensive fatigue data for AISI H11 for strain-rate controlled, low cycle fatigue at temperatures from 300°C to 600°C. (This temperature range contains the common friction stir welding temperatures for aluminum.) In these fatigue tests, there were three observed crack initiation locations: "non-metallic inclusions (NMI), lath boundaries, and grain boundaries of the initial austenitic microstructure." Quantification of these mechanisms led to the observation that NMI and lath boundary initiations completely dominated grain boundary initiations below 400°C. Grain boundary initiation "reach[ed] a proportion of 30% at 500°C, 65% at 550°C, and 90% at 600°C" (Velay 2005).

This observation of a transition in initiation mechanisms is significant because—though Velay *et al.* were studying H11 steel—the transition in mechanism corresponds to an observed transition in the rate of cyclic softening in a study of low cycle fatigue of H13 steel at elevated temperatures conducted by Engberg and Larsson. In their study, isothermal high-strain fatigue tests were conducted at 80, 300, 500, 600, and 750°C. Data from each of these tests was fit to a cyclic softening model, and the rate of cyclic softening from the model for each temperature was then graphed as a function of temperature (Engberg & Larsson 1988). The plotted "slopes" for each temperature can be interpreted as the rate at which cyclic softening occurs per strain cycle. Higher rates of cyclic softening correspond to shorter life, thus the higher the response, the fewer cycles to crack initiation and failure. As can be seen in the plot from Engberg and Larsson (Figure 2-1), they divided the softening into two regions, indicating that there is a sharp increase

in the cyclic softening when the temperature passes 430°C. This simply—yet significantly—indicates that there is a transition in high strain (LCF regime) cyclic softening of H13 steel when the operating temperature passes 430°C.

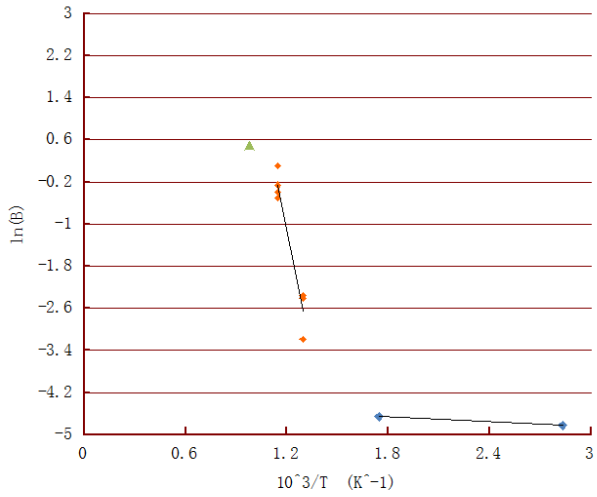

Figure 2-1: Rate of cyclic softening varying with temperature. B is the cyclic softening rate (Engberg and Larsson 1988)

It should be noted that cyclic softening behavior was also observed by Velay *et al.* in their study on H11 steel. They found that: "For the same strain ranges... An increase in temperature implies a decrease of stress level, a more important cyclic softening intensity and shorter lifetimes" (Velay 2005). Another important finding of this study was that there was no evidence of a creep mechanism during fracture analysis, despite choosing some test conditions purposely to induce creep. Though this study did not include H13 steel, the similarities between the two alloys suggest that it could be expected that crack propagation in H13 steel at elevated temperatures is similarly dominated by a fatigue mechanism, not a creep mechanism.

A very thorough study on fatigue of H11 was conducted by Denis Delagnes for his doctoral thesis (1998). This study focused on the fatigue behavior around the transition from the

low cycle fatigue regime (plastic strain dominated) to the high cycle fatigue regime (elastic strain dominated). This research included an in-depth study of the cyclic softening behavior, and—because the focus was on the LCF-HCF transition—Delagnes showed that cyclic softening is only significant in the low cycle fatigue regime. Delagnes also studied the effects of hardness and test temperature on fatigue life in this transition region. In examining the temperature effect on fatigue, the majority of failure data in Delagnes' study occurred between 4,000 and 50,000 cycles.

Basquin models (equation 1, where σ_a is the alternating stress, N is the fatigue life, and C_e and p are model parameters) were fit by Delanges to each temperature (see Figure 2-2), giving an independent stress-life relationship for each temperature. Then for each temperature, σ_a was

$$\sigma_a = C_e * N^p \quad (1)$$

solved for given N = 10,000 cycles and plotted against temperature (see Figure 2-3). From this plot, Delagnes identified a temperature transition in fatigue life behavior around 500°C. The previously mentioned transition in dominant crack initiation locations with temperature were given by Delagnes as the explanation for this transition in fatigue behavior. As this temperature transition was only studied at the LCF-HCF transition, a primary aim of this thesis is to determine whether such a transition exists in the high cycle fatigue range.

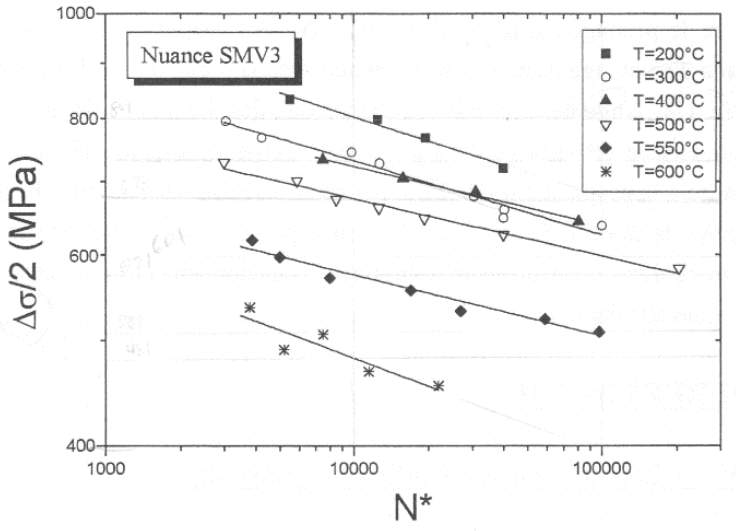

Figure 2-2: Basquin model fits of constant strain fatigue data from 200°C to 600°C. (Delagnes 1998)

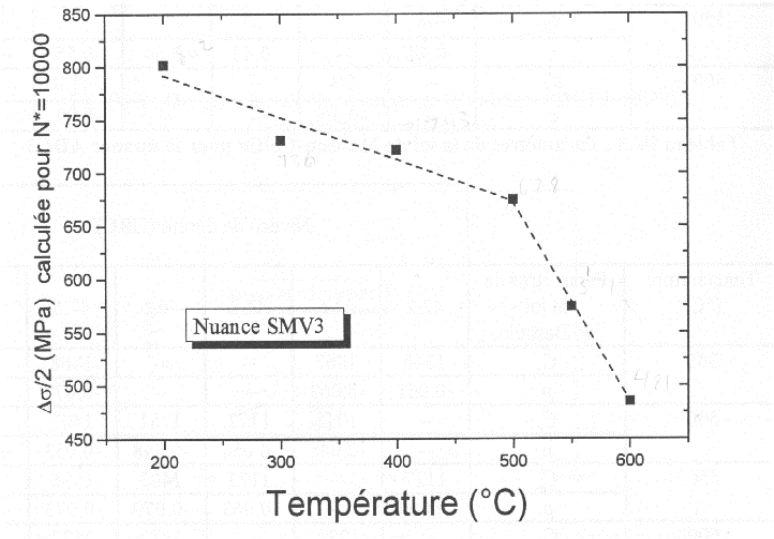

Figure 2-3: Stresses from Delagnes' Basquin fits of each temperature (Figure 2-2) at 10,000 cycles. (Delagnes 1998)

3 METHODOLOGY

To understand the effect of temperature on the fatigue life of H13, a rotating-bending fatigue experiment was conducted using a cantilever-beam bending fatigue machine at several temperatures. A pilot test was first conducted to estimate stress conditions that would yield failures in the high cycle fatigue regime—traditionally considered to be above 10^4 cycles. Following the pilot test, an in-depth study was conducted with 3 replicates at every test level.

3.1 Equipment and materials

The cantilever-beam rotating-bending fatigue machine used was a Fatigue Dynamics RBF-200. The RBF-200 is capable of rotating specimens at up to 10,000 rpm and is calibrated to provide a bending moment between 0 and 200 in-lbs. A built-in counter keeps track of the accumulated cycles and upon specimen breakage, the load drops and shuts off the machine. For temperature control, an electric resistance furnace was used in conjunction with a Love Controls Model 25013 temperature controller.

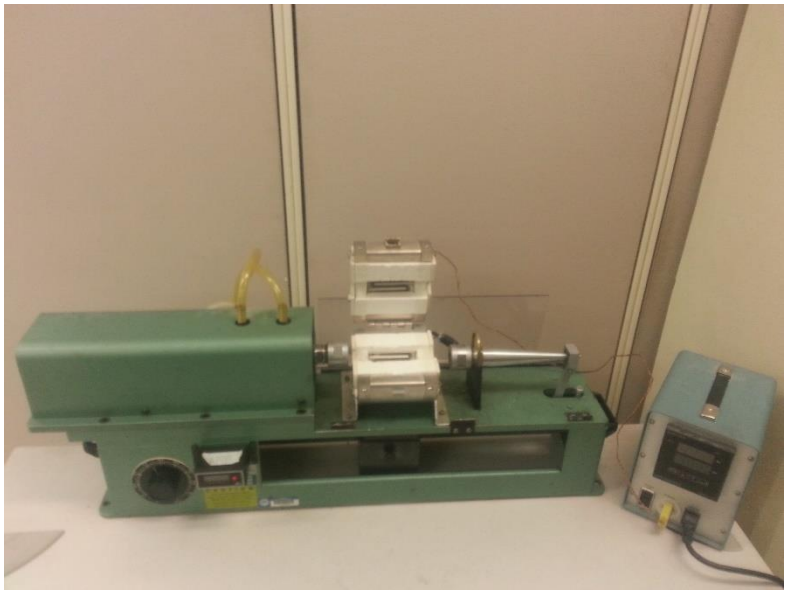

Figure 3-1: Rotating-bending fatigue machine with mounted furnace and adjacent temperature controller.

Specimens were designed as directed in the RBF-200 user manual and in accordance with ASTM E466, as far as permitted (Instruction Manual Model RBF-200; ASTM E466-07 2007). The drawing used for manufacturing is found in Appendix A. All specimens were heat treated, imbuing an average hardness of 48.7 HRC. The heat treatment followed these steps: specimens were first austenitized at 1015°C for 1 hour, then air cooled; tools were then tempered for 1 hour at 600°C, after which the furnace was turned off and allowed to cool with the parts inside. The heat treatment resulted in warping of several of the specimens, but they were straightened at elevated temperature (though below the tempering temperature) and any remaining runout was believed to be insignificant due to the loading method[1]. As the final step in the manufacturing process, the gauge section of each specimen was longitudinally ground to ensure a surface finish

[1] Because the rotating bending fatigue machine applies its load to the specimen via a single downward force and does not restrict the movement of the load point (see Figure 3-1) the loading is able to maintain a constant force, despite possible movement due to runout from the specimen.

of 8 μ-in R_a. This was in accordance with ASTM E466 and helped minimize surface finish effects on crack initiation (ASTM E466-07 2007).

3.2 Procedure

To ensure steady state temperature conditions, at the start of each testing period the system was pre-heated by running the furnace at 700°C for 1 hour with a dummy specimen installed. For each test, a thermocouple was secured onto the specimen just outside of the gauge section using fiberglass tape. The specimen was then mounted within the collets of the rotating bending fatigue (RBF) machine and the furnace closed around the specimen. The test specimen was then preheated for 10 minutes at 20°C above the test temperature—to reduce the time to achieve approximately steady state temperatures—following which the temperature was decreased to the test temperature. The thermocouple attached near the gauge section was used to monitor the stability of the actual specimen temperature, so as to gauge when an approximate steady state temperature was reached. After specimen temperature had reached steady state, the required load was applied and the RBF machine was turned up to 4500 rpm (±200 rpm to prevent resonance). Upon failure, the number of cycles to failure was recorded.

3.3 Temperature calibration

Meaningful analysis of the study results was highly dependent on accuracy of the test temperature. As indicated in Figure 3-2, the furnace controller received feedback via a thermocouple mounted through the outer wall of the furnace, positioned near the heating coils. Since the temperature at this position could not be assumed to coincide with the specimen temperature, it was necessary to measure the specimen temperature and calibrate it against the

furnace controller setpoint temperature. This calibration was first conducted using a thermocouple mounted at the smallest diameter point of the specimen gauge section using fiberglass tape (see Figure 3-2).

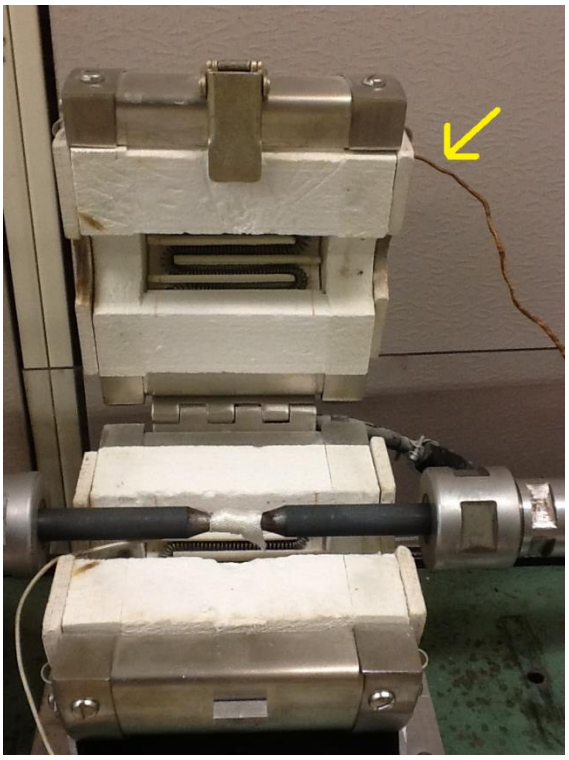

Figure 3-2: Thermocouple attached near minimum cross-section via fiberglass tape wrapping.

Following the pilot study, the temperatures were recalibrated using a thermocouple welded onto the gauge section (see Figure 3-3). Calibration data is given in Table 3.1, and plots of both calibrations are given in Figure 3-4, showing a distinct linear behavior. Testing temperatures were determined using the temperature calibration equation from the welded thermocouple measurements, which was considered more accurate because actual test specimens did not have fiberglass-wrapped gauge sections as did the specimens from the first calibration. It was not possible to determine the specimen temperature during actual testing due to the rotation

of the specimen, but it was assumed that changes in temperature due to rotation were insignificant. This assumption was justified by the fact that the during stationary heating, the specimen temperature was observed to increase significantly whenever the controller relay was on, thus suggesting that the radiative heat transfer dominated the convection heat transfer within the furnace.

Table 3.1: Furnace setpoint calibration comparing thermocouple attachment methods. (All temperatures are in °C)

Furnace Setpoint	Welded attachment	Fiberglass Wrapped Attachment	Welded/ Fiberglass Difference
403	300.2	296.8	3.4
487	399.8	391.5	8.4
571	499.5	486.1	13.3
614	550.5	534.6	15.9
656	600.3	581.9	18.4

Figure 3-3: Thermocouple attached near minimum cross-section via welding.

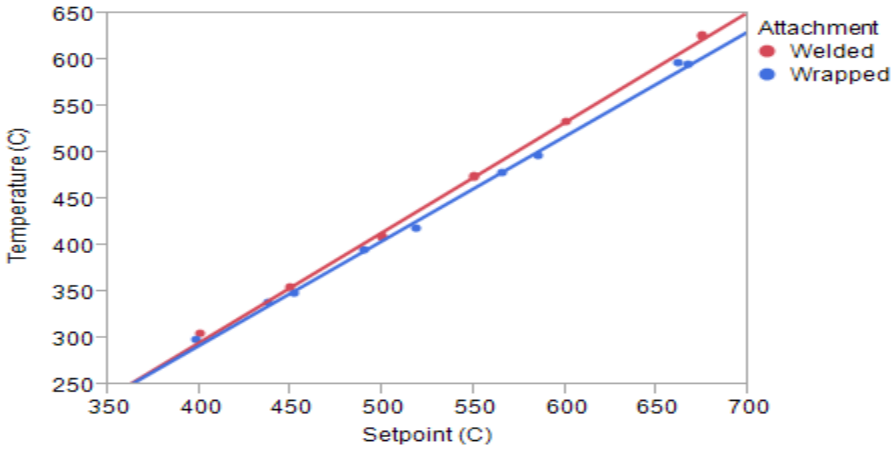

Figure 3-4: Temperature calibration plotting temperature measured on the specimen for thermocouples attached via wrapping with fiberglass tape ("wrapped") and welding ("welded"), as a function of furnace setpoint.

4 PILOT STUDY AND EXPERIMENTAL PLAN

An exploratory pilot study was conducted seeking to a) verify the testing methodology; b) see if the methodology gave repeatable results; and c) identify stresses at each temperature that lead to failures in the HCF regime. Fifteen specimens were used across five different temperatures, but a statistical experiment plan was not used, nor was the order of tests randomized (Table 4.1). The tests were conducted at furnace temperatures of 398, 452, 518, 585, and 667°C. With these furnace temperatures it was intended to obtain specimen temperatures of 300, 354, 419, 499, and 600°C, respectively, but the second calibration (see Calibration section for details) showed actual specimen temperatures to be 304, 362, 438, 560, and 619°C. Despite these differences, the results still provided useful information that was critical in designing the full study.

The pilot testing resulted in the previously discussed testing methodology, and repeatability of the results was taken as an indication of the soundness of the testing procedure (see results for testing at 438°C for 807 MPa and 878 MPa in Table 4.1). A Basquin model was fit to the results at each temperature, as was used by Delagnes for his S-N data (for Delanges plot, see Figure 2-2). While there were only two data points collected at 304°C and 560°C, and only 3 data points collected at 619°C, the Basquin model slopes at 304, 438, 560, and 619°C were all very similar, which suggested a consistent stress effect across all temperatures. While

this temperature-independent stress effect was not modeled in in the pilot study, in the full study such a temperature-independent stress effect was used in the fatigue life model and tested for statistical significance.

Table 4.1: Rotating bending fatigue life data from exploratory pilot study.

Pilot No.	Temperature (°C)	Stress (MPa)	Cycles
1	425	930	362300
2	425	807	1007800
3	425	878	117300
4	425	878	140500
5	425	807	1111100
6	425	843	280700
7	540	878	56800
8	540	728	1071500
9	595	878	3800
10	595	728	83400
11	354	965	444000
12	300	1088	24400
13	300	1009	83800
14	595	685	54400
15	354	1009	624900

When studying the effect of two different stresses on some response, a common approach to understanding the effect of one stress on the response (assuming independence) is to hold the other stress constant and look at the how the response varies as the free stress varies. This works well in understanding the effect of mechanical stress on fatigue life, as demonstrated by the Basquin model fits at each temperature. Unfortunately, to understand the effect of temperature on life, stress cannot simply be held constant as temperature varies. This was demonstrated by the testing that was done for 878 MPa at 438, 560, and 619°C: At this constant stress, the failure at 619°C occurred in the LCF regime, whereas the same stress at lower temperatures led to

failures in the HCF regime. This is consistent with the known yield strength behavior of H13 (Figure 4-1, from Philip's data): because the yield strength decreases dramatically above 425°C (see Figure 4-1), a stress that caused only elastic strain below 425°C, thus leading to high cycle fatigue—can induce plastic strain above 425°C—thus leading to low cycle fatigue. Delagnes' study demonstrated that a temperature effect on fatigue could be studied by holding fatigue life constant and seeing how mechanical stress varies as temperature varies : Obviously, fatigue life cannot be held constant in actual testing, but by constructing a Basquin model from fatigue data at two or more stress levels for each temperature, a stress can be calculated for each temperature at the same cycles to failure, thus synthesizing this stress-temperature relationship at constant fatigue life (see Figure 2-3 and the associated discussion on p. 7 to see how Delagnes' did this).

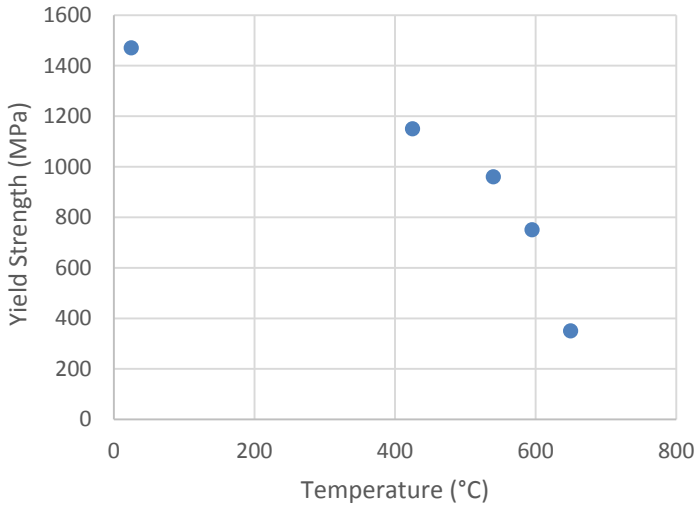

Figure 4-1: Yield strength at elevated temperatures of H13 tool steel tempered to a hardness of 48 HRC (Philip 1990).

Following Delagne's method, the Basquin models from the pilot study (Figure 4-2) were used to calculate the stress at $N = 5 \times 10^5$ cycles and $N = 10^6$ cycles for each temperature. The stresses at each temperature were then plotted as was done by Delagnes (see Figure 2-3), with

one difference: an inverse temperature scale and log stress scale were used on each respective axis (Figure 4-3). These scales were used in anticipation of an expected Basquin-Arrhenius model (see p. 23) that would be applied to the full study. From this plot, the stresses for the full study were chosen for each of the full study temperatures. (For ease of comparing the complete study results to the Delagnes' results, the test temperatures for the complete study were chosen to match the temperatures used by Delagnes: 300, 400, 500, 550, and 600°C.) Though the reader may question this method of selecting tests stresses, the degree of accuracy of this process is not important because all that was needed was to ensure that the high and low stress levels used in the full study would place failures in the high cycle fatigue regime at every temperature, preferably bracketing 10^6 cycles.

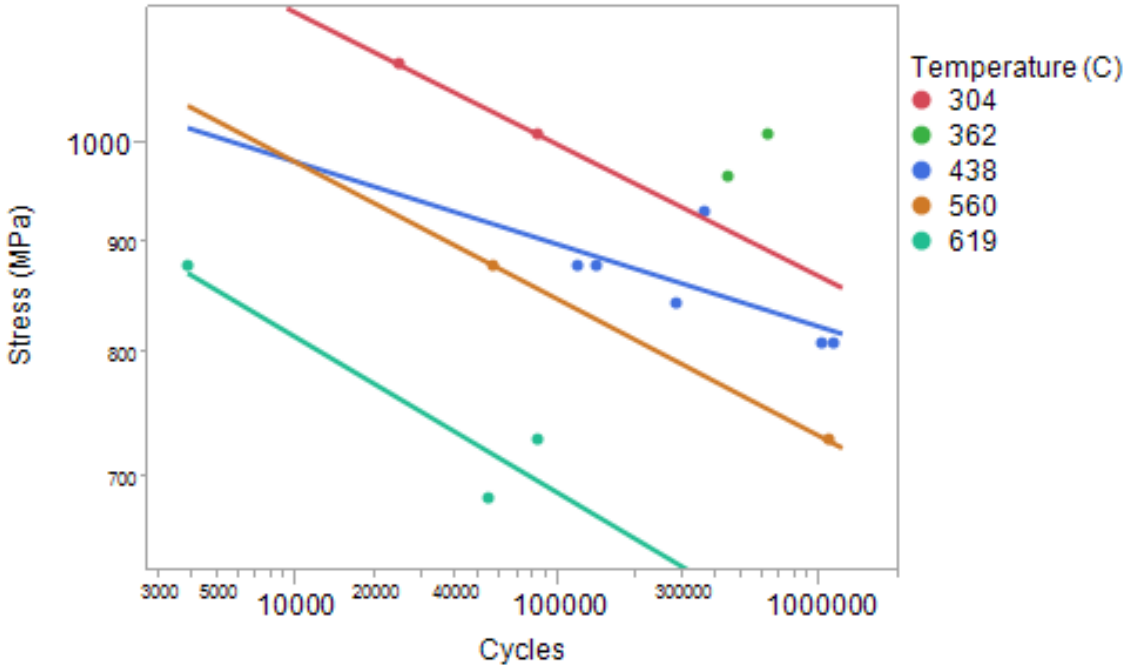

Figure 4-2: Basquin models were fit at each temperature for the pilot study data.

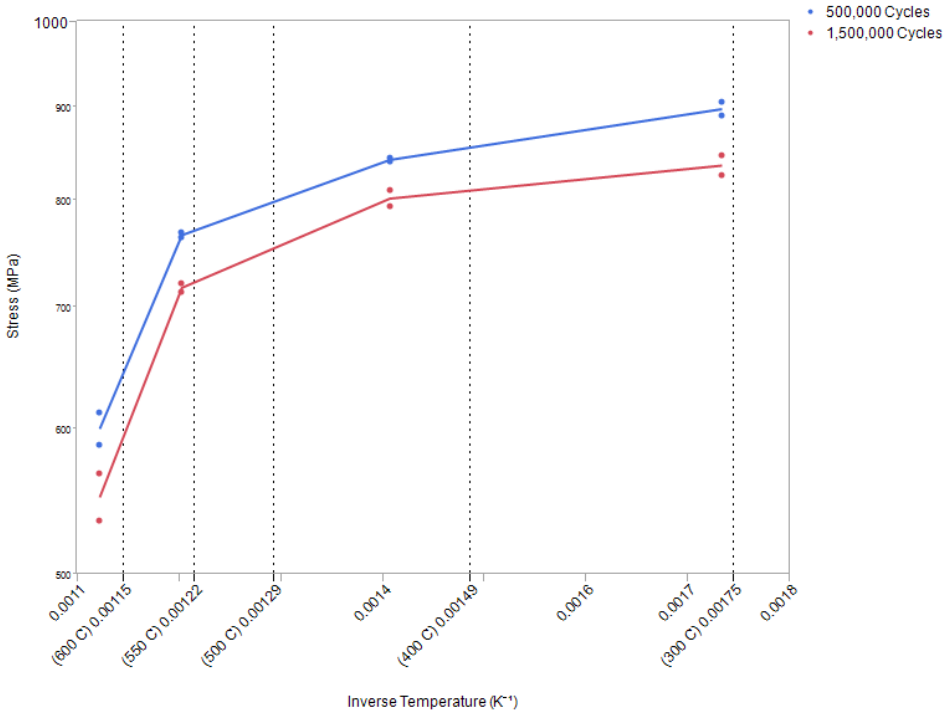

Figure 4-3: Stress estimates for $N = 5 \times 10^5$ cycles and $N = 10^6$ cycles from the pilot study data. Inverse temperature and log stress scales were used in anticipation of an expected Basquin-Arrhenius model (see p. 23). Dashed lines correspond to temperatures chosen for the full study.

5 RESULTS AND ANALYSIS

In analyzing the fatigue data from the full study, these steps will be taken:

1. A lognormal distribution will be found to provide the best model of the distribution
2. A Basquin model with categorical temperature effect will be introduced and fit to the fatigue data.
3. A continuous temperature effect (in the form of an Arrhenius model) will be proposed to replace the categorical temperature effect.
4. A temperature region effect will be added to the model to account for a transition in fatigue behavior.
5. Assumptions inherent to the model will be addressed an analyzed for their validity.

5.1 Distribution form

Because it is recognized that fatigue is a stochastic process rather than deterministic, the models for fatigue life need to also model the variation in fatigue life. For this purpose, parametric distributions are used to model the cycles to failure. Collecting nine data points at the higher stress level for 500°C provided sufficient data to estimate the form of the distribution for the cycles to failure. Fatigue data is traditionally fit using either a Weibull or lognormal distribution (Veers, 1996).To determine which lifetime distribution provided a better model of the data, both Weibull and lognormal distributions were fit to the 500°C data and goodness of fit

was compared. The relative likelihood of the lognormal distribution to the Weibull distribution was found to be 3.00 (equation 2), indicating that the lognormal distribution is 3.00 times as likely to minimize information loss due to modeling compared to the Weibull distribution. The relative likelihood was calculated using AICc (Akaike Information Criterion with correction), which is a measure of how effective a model is at capturing all the information available in a dataset. The AICc for the Weibull and lognormal fits were calculated to be 252.7 and 250.5, respectively.

$$\exp\left(\frac{252.7 - 250.5}{2}\right) = 3.00 \qquad (2)$$

Figure 5-1(a) shows the 500°C data on a Weibull probability plot and (b) shows the data on a lognormal probability plot. As demonstrated by the relative likelihood calculation, the data plotted on the lognormal probability plot more closely follows the parameter estimate line than the data on the Weibull plot follows the parameter estimate line. Neither the graphic evaluation, nor the relative likelihood definitively indicate a "correct" model, they just indicate that the lognormal distribution is more likely to capture more of the information in the data.

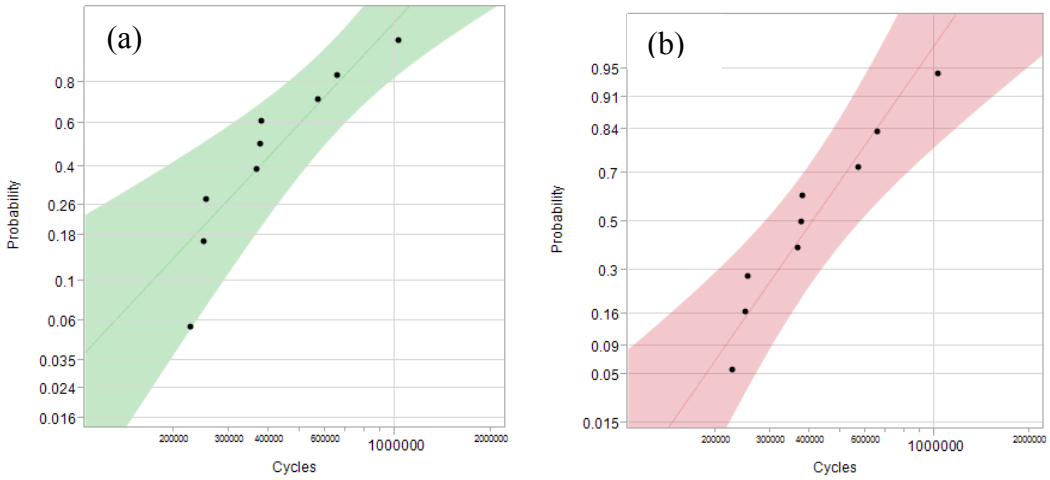

Figure 5-1: The data collected at 500°C and 816 MPa on (a) a Weibull probability plot and (b) a lognormal probability plot. The lognormal model provides a better fit.

Model fitting was conducted in the statistics program JMP using maximum likelihood estimation (MLE). This method of model parameter estimation has a number of advantages over least squares estimation. Generally, though, it provides a statistically more accurate estimate of parameters and utilizes more of the information available in the data (Tobias & Trindade 2012). In the MLE method, parameters are estimated by maximizing the likelihood function, which represents the likelihood of the estimated parameters being the best fit, given all the data. The value of the maximized likelihood function is called the likelihood.

The models for fatigue life presented in this study all follow a lognormal distribution, unless otherwise stated, and therefore all modeled cycles to failure are the median cycles to failure for the given conditions (which—for the lognormal distribution—is equivalent to the mean of the natural logarithm of the cycles to failure). Though not presented with every model, the scale parameter, σ—which accounts for the variance in fatigue life—is inherent to the lognormal distribution and is given in this study where relevant. (Figure 5-2 provides a graphic representation of the distribution and its variance.) For the lognormal distribution, the scale parameter can be interpreted as the standard deviation of the natural logarithm of the cycles to failure.

5.2 Stress effect modeling

A model was developed seeking to account for both the effect of stress as well as the effect of temperature on the fatigue life of H13. To account for the stress effect, a Basquin model (equation 3) was chosen, since this is a commonly used fatigue model (Veers 1996) and Delagnes used this model for the S-N data in his H13 fatigue study (see equation 1). For this study the Basquin model was used in the form of equation 3, where N is the cycles to failure

(actually the median cycles to failure or 50th percentile, since this follows a lognormal distribution), S_a is the stress amplitude (σ is reserved to denote the lognormal scale parameter instead of stress), and S_0 is a normalization factor (1 MPa) to ensure correct units and C and b are the model parameters. Note that this is just a rearrangement and re-parameterization of the Basquin model as used by Delagnes (equation 1).

$$N = C * \left(\frac{S_a}{S_0}\right)^b \tag{3}$$

Equation 3 is only valid at constant temperature conditions. To evaluate the fit of the Basquin model to the fatigue data across *all* temperatures, a categorical temperature effect was added to the model. Treating the temperature effect as categorical allows the temperature effect to be accounted for without assuming a form for the life-temperature relationship. The natural logarithm of this model is expressed as

$$\ln(N) = \ln(C) + b \ln\left(\frac{S_a}{S_0}\right) + a_{T_i} \tag{4}$$

where 'a_{Ti}' is the temperature effect for the i^{th} temperature. Whereas equation 3 must be fit at each temperature—and therefore gives different estimates of C and b (and the scale parameter, σ) at each temperature—equation 4 provides a pooled estimate of C, b and σ across all temperatures. The fit of the data at 400°C using equation 4 is depicted in Figure 5-2. To test the statistical significance of the model, a likelihood ratio test was used. The likelihood ratio test compares the likelihood of the given model with the likelihood of the same model, but with the term being tested excluded; the test results in a p-value that indicates the probability that the model with the effect is statistically the same as the model without the effect. Using this test, both the stress effect and categorical temperature effects were significant (Table 5.1). Despite the

statistical significance of the model effects, the model is impractical since it ignores the continuous nature of temperature.

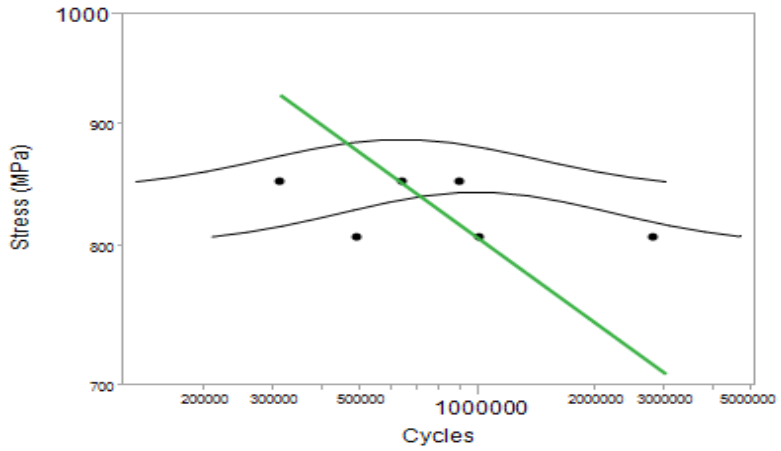

Figure 5-2: The Basquin model fit of the 400°C data showing the probability density function at the two stress levels. The fit line passes through the median cycles to failure at each stress level.

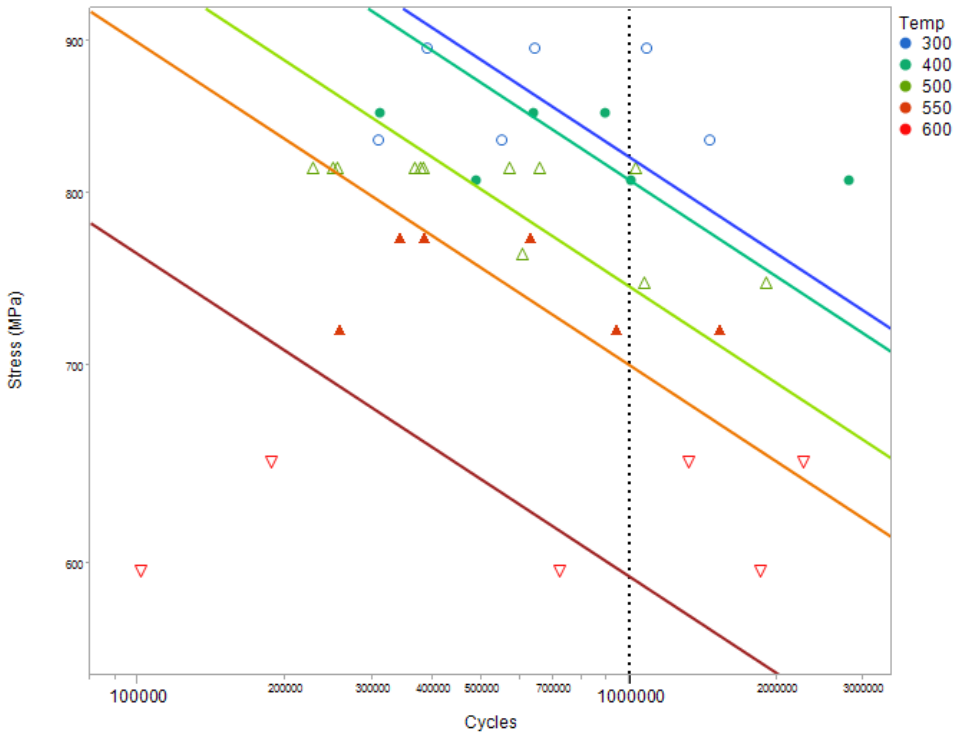

Figure 5-3: The Basquin model fit with the pooled stress effect as indicated by the constant slope across all temperatures. The line at 10^6 cycles identifies the stresses plotted in Figure 5-4 at each temperature.

Table 5.1: Model effects from the pooled Basquin model with categorical temperature effects. (see equation 3). 'L-R ChiSquare' is the likelihood ratio test statistic and 'Prob>ChiSq' is the p-value for the given statistic.

Effect	L-R ChiSquare	Prob>ChiSq	Estimate
ln(*C*)	16.10451	<0.0001	69.38544
b	11.30586	0.0008	-8.454308
Categorical Temperature	*35.65891*	*<0.0001*	
300			*1.142873*
304			*0.130793*
362			*2.079574*
400			*1.010041*
438			*0.470175*
500			*0.276165*
550			*-0.23228*
600			*-0.46029*
619			*0.00*

With the purpose of getting to a continuous temperature effect, equation 4 is rewritten to express stress as a function of fatigue life and temperature (equation 5). As addressed in the pilot study, it is impossible to conduct fatigue tests at constant stress across all temperatures, because the temperature effects on fatigue would cause failures at high temperatures to occur in the low cycle fatigue regime. By expressing stress as a function of temperature it is easier to examine the temperature effect, since stress as a function of temperature can be plotted for a constant fatigue life, as is done in Figure 5-4(a).

$$\ln\left(\frac{S_a}{S_0}\right) = \frac{\ln(N) - \ln(C)}{b} - \frac{a_{T_i}}{b} \tag{5}$$

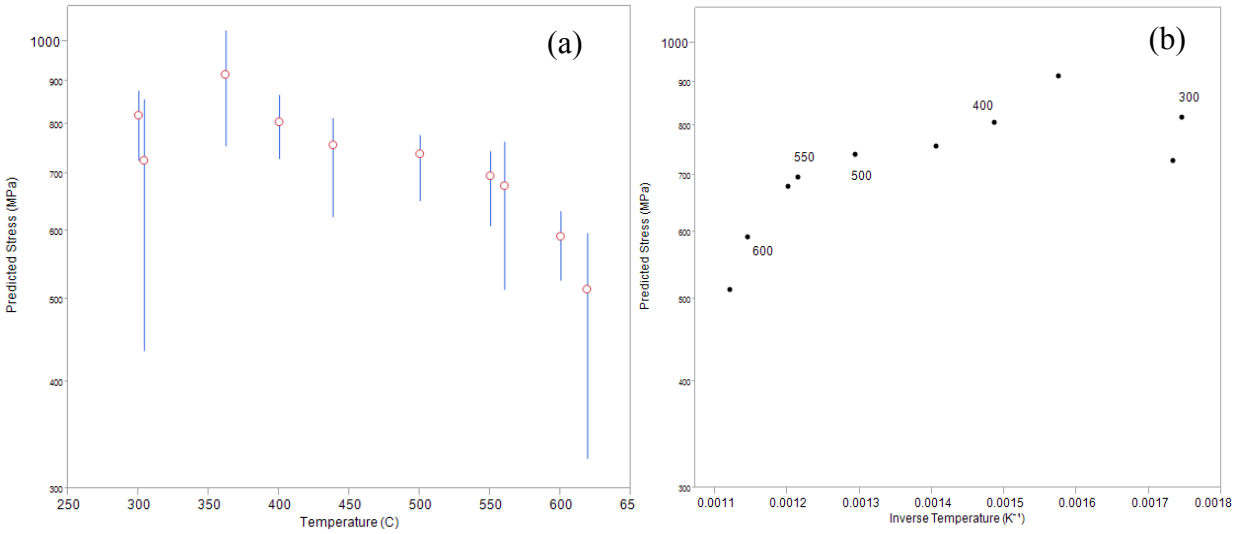

Figure 5-4: From the Basquin model fit with categorical temperature effects (equation 5) with the stress predicting a fatigue life of 10^6 cycles plotted for each temperature. (a) 95% confidence intervals are shown. (b) The stresses are plotted against inverse temperature. Individual labels are in °C.

5.3 Temperature effect modeling

Figure 5-4(a) plots the stress-temperature relationship at 10^6 cycles to failure. It is important to emphasize that the points on this plot do not represent actual failures, but rather are points from solving equation 5 for each temperature, hence the 95% confidence intervals. Figure 5-4(b) plots the same data using inverse temperature on the abscissa. Inverse temperature was used because it is consistent with an Arrhenius model of the temperature effect: Schuchtar used an Arrhenius relationship to model the effect of temperature on fatigue crack propagation (da/dN) in H13 (Schuchtar 1988) and the Arrhenius relationship is a commonly used model for accelerating failures with respect to temperature in other reliability studies (Nelson, 1990; Tobias & Trindade, 2012). The Arrhenius relationship can replace the categorical temperature effect by substituting equation 6 into equation 4, giving equation 7, where T is the temperature in Kelvin, R is the universal gas constant, and Q is the activation energy.

$$a_{T_i} = \frac{Q}{RT} \tag{6}$$

$$\ln(N) = \ln(D) + b * \ln\left(\frac{S_a}{S_0}\right) + \frac{Q}{RT} \tag{7}$$

Equation 7 is in log form, and can be expressed in its base form as:

$$N = D * \left(\frac{S_a}{S_0}\right)^b * \exp\left(\frac{Q}{RT}\right) \tag{8}$$

Or equation 7 can be rearranged to give the relationship in equation 9, which could also be considered a substitution of the Arrhenius relationship into equation 5.

$$\ln\left(\frac{S_a}{S_0}\right) = \frac{\ln(N) - \ln(D)}{b} - \frac{Q}{bRT} \tag{9}$$

Figure 5-4(b) provides a plot of the relationship from equation 9 at a constant fatigue life of $N = 10^6$ cycles. The plot suggests that there is not a linear relationship between the natural log stress and the inverse temperature; however, it can be seen that there are two approximately linear temperature segments: one region being from 300°C to 500°C, the other region being 550°C to 619°C. To account for this two-region behavior, a temperature region indicator effect (G_{temp}) is added to the model along with an inverse temperature-temperature region interaction effect, giving equation 10. The logarithmic form, equation 11, was the form used in JMP to calculate the MLEs of the model parameters. By combining the temperature region indicator effect and its associated interaction effect with their respective similar terms in the model, equation 10 can be replaced with a piecewise equation—one portion for each temperature region—in the form of equation 8. Thus the final two-region Basquin-Arrhenius model estimates

calculated using equation 11 are given in the form of the piecewise equation 12. The complete study results are compared to the two-region Arrhenius model predictions for the given test conditions in Table 5.3.

$$N = D * \left(\frac{S_a}{S_0}\right)^b * \exp\left(G_{temp[0/1]}\right) * \exp\left(\frac{Q}{RT}\right) * \exp\left(\frac{Q}{RT} * G_{temp[0/1]}\right) \quad (10)$$

$$\ln(N) = \ln(D) + b * \ln\left(\frac{S_a}{S_0}\right) + G_{temp[0/1]} + \frac{Q}{RT} + \frac{Q}{RT} * G_{temp[0/1]} \quad (11)$$

$$\begin{aligned} N &= \exp(72.32) * \left(\frac{S_a}{S_0}\right)^{-9.2} * \exp\left(\frac{16031\ \text{J/mol}}{RT}\right) \qquad T < 537°\text{C} \\ N &= \exp(43.91) * \left(\frac{S_a}{S_0}\right)^{-9.2} * \exp\left(\frac{206944\ \text{J/mol}}{RT}\right) \quad T > 537°\text{C} \\ \sigma &= 0.773 \end{aligned} \quad (12)$$

The two-region model identified 537°C as the transition temperature and indicated that the change in activation energy was non-trivial. Table 5.2 provides the results of the likelihood ratio tests from JMP, indicating that all model terms were significant. Figure 5-5 shows the two-region Arrhenius model (taking the form of equation 9 to express stress as the dependent variable) superimposed on the plot from Figure 5-4. It is important to note that data from the pilot study was included in this analysis. Because the order of tests in the pilot study was not randomized, it is possible that this data introduces some biasing into the model, but it was assumed that the effect of any biasing would be outweighed by the increased accuracy of the model.

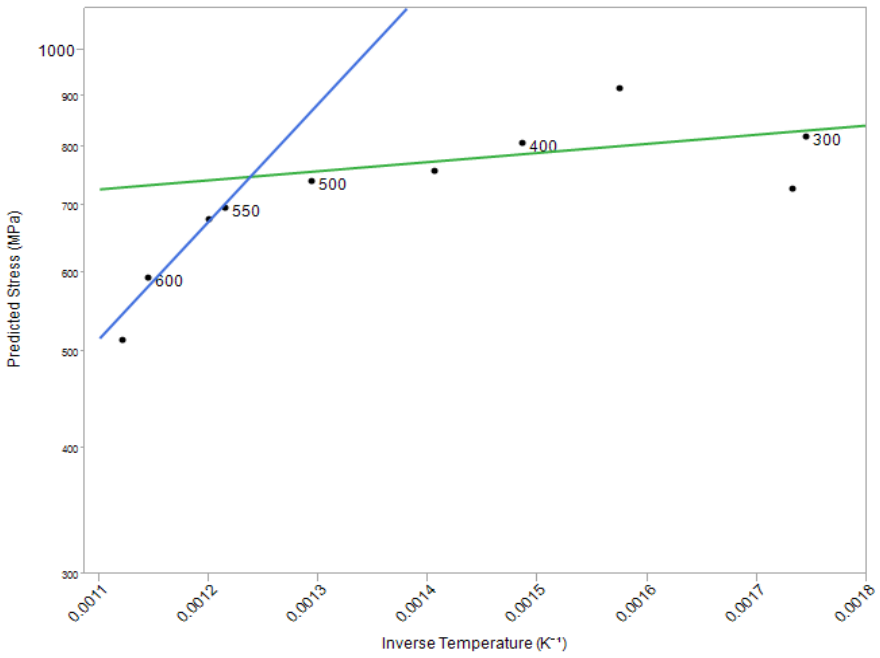

Figure 5-5: The two-region Arrhenius model relating the stress predicting a fatigue life of 10^6 cycles as a function of inverse temperature (see equations 9 & 12). Individual labels are in °C.

Table 5.2: Model effects from the combined Arrhenius-Basquin model. (see equation 7)

Effect	L-R ChiSquare	Prob>ChiSq
b	26.359111	<.0001*
Q/R	15.536849	<.0001*
G_{temp}*Q/R	13.468139	0.0002*
G_{temp}	7.6531044	0.0057*

Table 5.3: The complete study data and the associated estimated median fatigue life (Predicted Cycles) from the Arrhenius-Basquin model (Equations 12) for the given temperature and stress.

Temperature (°C)	Stress (MPa)	Actual Cycles to Failure			Predicted Cycles
		Specimen 1	Specimen 2	Specimen 3	
300	834	308 400	1 455 600	549 200	943 851
300	895	1 086 000	388 100	643 100	490 651
400	807	487 100	2 805 000	1 005 000	769 308
400	851	894 600	637 100	310 700	472 714
500	746	1 067 900	1 892 600		1 100 198
500	764	605 700*			888 232
500	816	254 100	653 800	226 600	480 837
		1 025 700	569 900	380 200	
		248 600	365 200	374 700	
550	720	257 600	1 531 700	942 900	832 235
550	772	383 300	342 300	631 300	434 537
600	597	101 000	1 850 400	718 800	824 911
600	649	2 261 900	1 322 600	186 100	378 859

***After one specimen was run to failure at 500°Cand 764 MPa, the "low" stress level for 500°C was decreased to 746 MPa to ensure failures well beyond those at the "high" stress level**

Model assumptions

In generating this model, there were a few important assumptions made. One important assumption was that the model had constant variance. The residuals by predicted value plot (Figure 5-6(b)) bears out this assumption; since the residuals are evenly distributed above and below zero, they appear randomly scattered and they display no visible bias or trend. The only exceptions might be from the data collected at 600°C, which appears to have a larger variance (Figure Figure 5-6(a)).

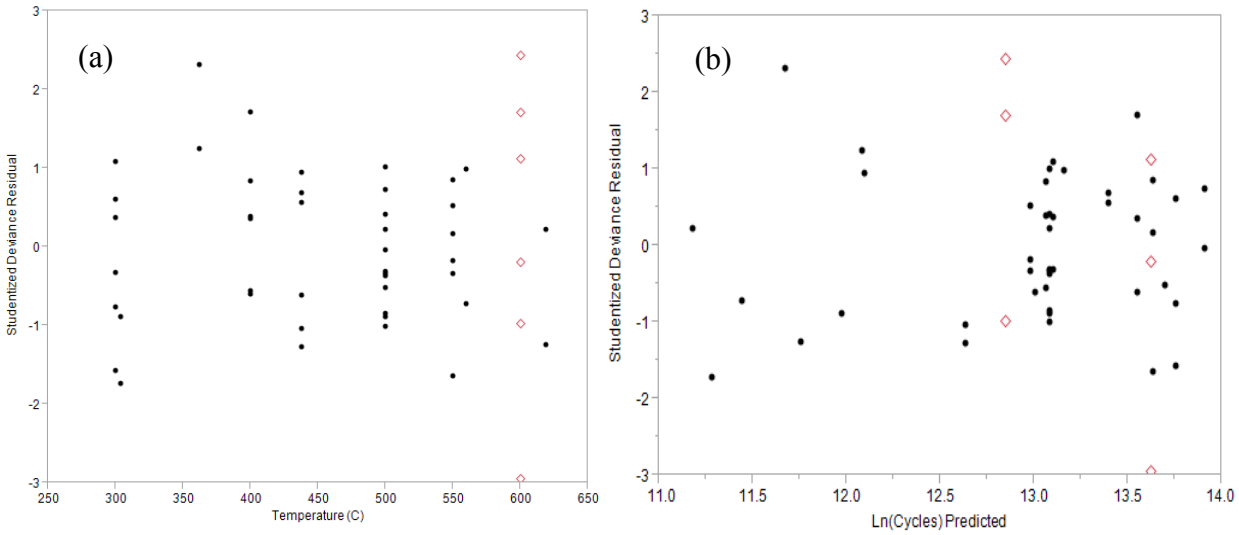

Figure 5-6:Studentized devianace residuals from the two-region Arrhenius model, (a) plotted by temperature and (b) plotted by predicted Ln(Cycles). Residuals from tests at 600°C are given as red diamonds.

To further explore the observed variance 600°C a simple Basquin model was fit at each temperature (equation 3). From these individual Basquin fits the estimated scale parameter at 600°C, $\sigma = 1.14$, was approximately twice the value at the other temperatures (see Table 5.4). A possible explanation for this increased variation is that at 600°C the uncertainty of the applied stress (which is assumed to be constant across all temperatures) is a greater portion of the applied stress, since the applied stress decreased as temperature increased. Thus the uncertainty of the applied stress became a larger contributor to the variance of the fatigue life. This explanation is inadequate by itself though, because if this were the case, it would be expected to see a growth in variance as temperature increases, which is not demonstrated in Figure 5-6(a).

Table 5.4: The scale parameter for the lognormal distribution from individual Basquin models fitted at each temperature. The scale parameter estimate for 600°C is about twice the size of the scale parameter at any of the other temperatures.

Temperature (°C)	σ Estimate	Lower 95%	Upper 95%
300	0.5416	0.2352	0.8480
400	0.5959	0.2588	0.9331
500	0.4476	0.2685	0.6266
550	0.5644	0.2450	0.8837
600	1.1444	0.4969	1.7919

Another possible contributor to this increased variation is that at 600°C both stress levels were very near the fatigue limit. Research by Kazymyrovych (2010) indicates that there is not a "true" fatigue limit for H13 in the sense that below the fatigue limit life is not infinite, but there is a transition to a no longer linear log-Stress-log-Life relationship as demonstrated by Kazymyrovych's plot in Figure 5-7. Operating near the fatigue limit would greatly increase the variation of the time to failure, which would be consistent with the greatly increased variance estimated at 600°C.

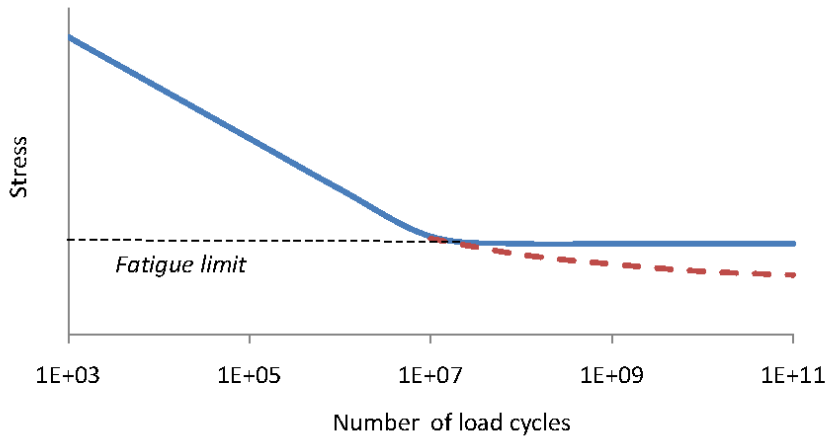

Figure 5-7: H13 does not have a "true" fatigue limit (the curve follows the dashed line). (Kazymyrovych 2010)

6 DISCUSSION

6.1 The loading method

Before comparing the results of this study with other published findings, it is important to examine the experimental setup and discuss the differences and commonalities it has with other studies. The Delagnes' study (1998) has the most in common with this study, but there are several key differences. The first is that his Basquin modeling was conducted on H11 with a hardness of 42 HRC, compared to the H13 with an average hardness of 48.7 HRC used in this study. Delagnes' specimens were subjected to uniaxial stress, whereas this study used rotating bending stress. In rotating bending loading, only the outermost surface is subject to the maximum stress, while uniaxial fatigue subjects the entire cross-section to a uniform maximum stress. The differences in loading necessarily imply fewer cycles to crack initiation in the uniaxial loading, since the increased area under stress means there are more sites available for crack initiation.

Takai et al. suggested that rotating bending loading is actually very similar to the loading conditions experienced by FSW tools: "It is likely that a torsional load from the rotational torque is applied on the actual tool in addition to that noted above [the bending load] but when the pin fracture surface is observed the fracture is at a right angle to the central axis and therefore [it is assumed]... the effect of torsional stress is small" (Takai et al. 2007). Based on Takai's

observation of tool fracture surfaces, we are inclined to accept that the torsional stress effect is small. In such a case, the rotating bending loading does a good job modeling the majority of the actual loading conditions on the FSW tool.

Another important difference in the loading is that Delagnes used constant strain loading, whereas this study used constant stress loading. Delagnes conducted constant strain cycling in the LCF-HCF transition region. Because Delagnes' tests were in this region, cyclic softening occurred in his specimens, meaning that the stress actually decreased during his constant strain tests (1998). In this study, testing was in the HCF regime meaning stresses were low enough that no cyclic softening occurred.

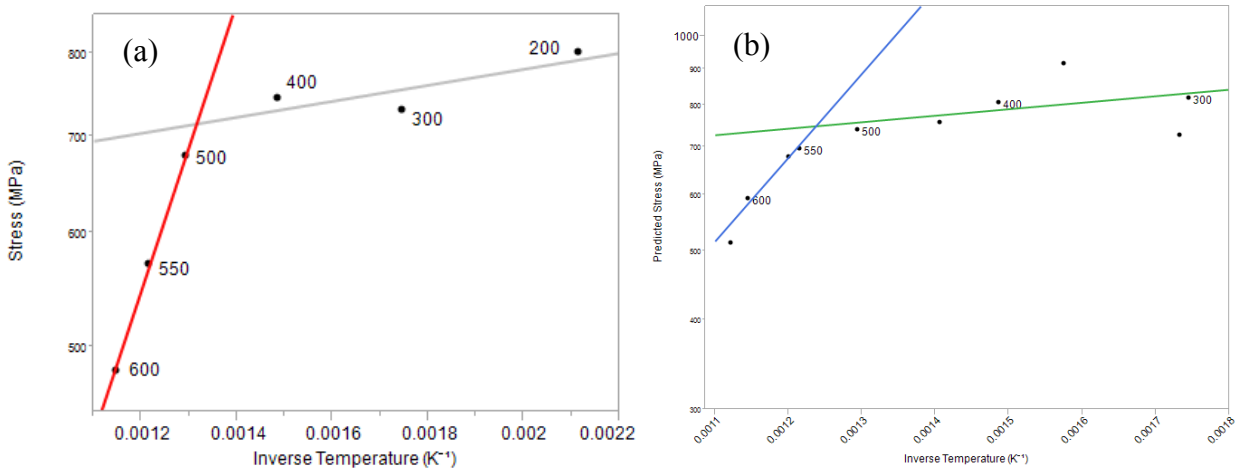

Figure 6-1: (a) A log-stress-inverse temperature model (equation 13) applied to Delagnes' 10,000 cycle stress estimates (see Figure 2-3). (b) The two-region Arrhenius model relating the stress predicting a fatigue life of 10^6 cycles as a function of inverse temperature (see equations 9 & 12). (Individual labels are in °C.)

6.2 Comparison with other study results

It is of note that the activation energy for the low temperature region is consistent with activation energies calculated for H13 by Schuchtar (1988). In his study he was looking at crack propagation rates of H13 at elevated temperatures between 300°C and 500°C, using an Arrhenius

modification of the traditional Paris crack growth equation. Schuchtar found activation energy of two different variants of H13 to be 13,000 J/mol and 17,000 J/mol, which is relatively close to the 16,031 J/mol activation energy identified in this study. The activation energy indicates how much the cycles to failure changes with an associated change in temperature. Below 537°C, in the low temperature region, when the inverse temperature decreases by 2.176E-5 K^{-1} (approximately a 10°C increase around 400°C) the fatigue life decreases by 4.1%. In the high temperature region, above 537°C, when the inverse temperature decreases by the same amount (approximately a 15°C increase around 550°C), the fatigue life decreases by 41.8%. The obvious implication for friction stir welding is that this suggests tool reliability dramatically drops in the high temperature region.

$$\ln\left(\frac{S_{N=10,000}}{S_0}\right) = y + \frac{M}{T} \tag{13}$$

Because Delagnes' Basquin model didn't use a single stress effect across all temperatures as was done in this study, the same evaluation cannot be made from his data about the temperature effect on fatigue life, but it is possible compare the temperature effect on stress at a constant life between the two studies. Delagnes didn't attempt to model the temperature effect, but graphically identified it as occurring around 500°C (see Figure 2-3). By replotting the data from Figure 2-3 on log stress and inverse temperature axes, equation 13 can be fit to Delagnes' estimates of stress leading to a fatigue life of 10,000 cycles ($S_{N=10,000}$), for a high temperature region and a low temperature region. It is important to remember that this is a fit of Delagnes' modeled points ($S_{N=10,000}$), and not Delagnes' actual fatigue test data. Using this method, the temperature transition is found to occur at 488°C.

From the Delagnes' fit (Figure 6-1(a)), below 488°C, when the inverse temperature decreases by 2.176E-5 K^{-1} (approximately a 10°C increase around 400°C) the stress leading to a median life of 10,000 cycles decreases by 0.28%. Above 488°C, when the inverse temperature decreases by the same amount (approximately a 15°C increase around 550°C), the stress leading to a median life of 10,000 cycles decreases by 4.90%. From this study's two-region Arrhenius model (Figure 6-1(b)), below 537°C, when the inverse temperature decreases by 2.176 E-5 K^{-1} (approximately a 10°C increase around 400°C) the stress leading to a median life of 10^6 cycles decreases by 0.45%. Above 537°C, when the inverse temperature decreases by the same amount (approximately a 15°C increase around 550°C), the stress leading to a median life of 10^6 cycles decreases by 5.71%. Despite the differences in the transition temperatures, for the high temperature and the low temperature region from both models, temperature effect on stress at a constant life is very similar.

It is important to acknowledge that the transition in the Arrhenius temperature effect is likely not abrupt, despite using an abrupt transition model in this study. The transition in activation energy is possibly the result of the increase in grain boundary crack initiation identified by Delagnes in his doctoral research (Delagnes, 1998) and quantified by Velay (Velay 2005) (see p. 5). The data indicates that the transition between the two linear regions is clearly not as abrupt as the model indicates (Figure 6-1(b)), which is consistent with the gradual growth in prevalence of grain boundary initiations. Taking into account the likely gradual nature of the transition in temperature effect, it is possible that the transition observed at 10^4 cycles (modeled as occurring at 488°C) and the transition observed at 10^6 cycles (modeled as occurring at 537°C) are one and the same.

Having identified two regions of fatigue behavior, it is important to revisit some of the model assumptions to see if they are still valid. When there is a transition in failure mode, the variance of life distribution can often change (Hu, Barker, Dasgupta, & Arora 1992). The constant variance used in the model is therefore brought into question. Such a transition in model variance could also be a reason for the significantly higher variance in the data collected at 600°C. Despite this possible deficiency in the model, from the perspective of friction stir welding, the most important conclusion is unaffected: fatigue life dramatically decreases at temperatures above approximately 500°C.

7 CONCLUSION

This study has demonstrated that there is a large temperature effect in high cycle fatigue of H13 tool steel. Near 537°C there is a transition in temperature effect, and above this transition the temperature effect on fatigue life is almost 10 times the size of the temperature effect below the transition. The implication for friction stir welding is that accelerated testing of FSW tools should be conducted below 500°C to stay in the same failure mode. This in turn suggests that a temperature control methodology (such as the method suggested by Ken Ross (Ross 2012)) should be used to control welding to ensure temperatures stay below this safe limit. Though the differences between this study and Delagnes' study of constant strain fatigue of H11 in the vicinity of fatigue life of 10,000 cycles present some uncertainties, the similarities in the results suggest that the temperature effect transition is the same (approximately 500°C) for high cycle fatigue (~10^6 cycles) and the low cycle to high cycle fatigue transition (~10^4 cycles). Thus, the temperature effect transition can be assumed to be independent of mechanical stress, and friction stir welding temperatures should be kept below the transition temperature, regardless of weld speed or tool stress.

8 FUTURE WORK

For the consideration of tool fatigue of H13 tools in friction stir welding, this research has already determined important constraints on welding temperatures, but to predict fatigue life of in-use tools, a fatigue study should be carried out on actual tools. This study has provided a foundation for predicting tool life based on bending stresses that will provide guidance for selecting welding parameters in an actual tool fatigue study.

Since this study conducted bending on 0.200” diameter specimens, the fatigue life relationships found herein are only useful for the same dimensions in bending fatigue, though the activation energies for the temperature effect are valid regardless of geometric factors. An important step in expanding these relationships to more friction stir welding tools would be to determine a geometry relationship that accounts for the change in fatigue life associated with a change in specimen/tooling diameter and stress concentration factors. With further research in fatigue of friction stir welding tools, a foundation will be established for maximizing tool usage while minimizing in-use tool failures, thereby reducing welding costs and making friction stir welding a more attractive manufacturing method.

REFERENCES

Andrews, R. E. "Improvements in Friction Stir Welding Tool Technology." *TWI Industrial Member Report Summary 1046*. TWI, 2013.

ASTM E466-07. *Standard Practice for Conducting Force Controlled Constant Amplitude Axial Fatigue Tests of Metallic Materials.* West Conshohocken, PA.: ASTM International, 2007.

Arora, A., M. Mehta, A. De and T. DebRoy. "Load Bearing Capacity of Tool Pin During Friction Stir Welding." *International Journal of Advanced Manufacturing Technology* 61, (2012): 911-920.

Colegrove, P. A. and H. R. Shercliff. "Experimental and Numerical Analysis of Aluminium Alloy 7075-T7351 Friction Stir Welds." *Science & Technology of Welding & Joining* 8, (2003): 360-368.

DebRoy, T., A. De, H. K. D. H. Bhadeshia, V. D. Manvatkar and A. Arora. "Tool Durability Maps for Friction Stir Welding of an Aluminium Alloy." *Proceedings of the Royal Society A: Mathematical, Physical and Engineering Science* 468, (2012): 3552-35700

Delagnes, Denis. "Comportement Et Tenue En Fatigue Isotherme D'aciers a Outils Z38 Cdv5 Autour De La Transition Fatigue Oligocyclique-Endurance." Doctoral, Ecole Nationale Supérieure des Mines de Paris, 1998.

Engberg, G. and L. Larsson. *Elevated-Temperature Low Cycle and Thermomechanical Fatigue Properties of Aisi H13 Hot-Work Tool Steel*. ASTM, 1988. Text.

Fernandez, G. J. and L. E. Murr. "Characterization of Tool Wear and Weld Optimization in the Friction-Stir Welding of Cast Aluminum 359+20% Sic Metal-Matrix Composite." *Materials Characterization* 52, no. 1 (2004): 65-75.

Hu, J. M., D. B. Barker, A. Dasgupta and A. K. Arora. "Role of Failure-Mechanism Identification in Accelerated Testing." In *Reliability and Maintainability Symposium, 1992. Proceedings., Annual*, 181-188, 1992.

"Instruction Manual Model RBF-200 Rotating Beam Fatigue Testing Machine. " Dearborn, Mich.: Fatigue Dynamics Inc.

Kazymyrovych, Vitaliy. "Very High Cycle Fatigue of Tool Steels." Doctoral, Karlstad University, 2010.

Nelson, Wayne. *Accelerated Testing : Statistical Models, Test Plans and Data Analyses*. New York: Wiley, 1990.

Philip, T.V. and T.J. MCaffrey. "Ultrahigh-Strength Streels." In *Properties and Selection: Irons, Steels, and High-Performance Alloys*, 1, 430-448: ASM International, 1990.

Prado, R. A. Murr L. E. Soto K. F. McClure J. C. "Self-Optimization in Tool Wear for Friction-Stir Welding of Al 6061+20% Al2o3 Mmc." *MATERIALS SCIENCE AND ENGINEERING A* 349, no. 1/2 (2003): 156-165.

Rai, R., A. De, H. K. D. H. Bhadeshia and T. DebRoy. "Review: Friction Stir Welding Tools." *Science & Technology of Welding & Joining* 16, (2011): 325-342.

Ross, Kenneth A. "Investigation and Implementation of a Robust Temperature Control Alogorithm for Friction Stir Welding." Brigham Young University, 2012. Retrieved from http://scholarsarchive.byu.edu/etd/3919 (3919)

Schuchtar, E. "Temperature Dependence of Fatigue Crack Propagation in Hot Work Die Steels." *Theoretical and Applied Fracture Mechanics* 9, no. 2 (1988): 141-143.

Takai, H., M. Ezumi, K. Aota and T. Matsunaga. "Basic Study of Friction Stir Welding Tool Life-Investigation for Increase of Fsw Reliability." *Welding International* 21, no. 9 (2007): 621-625.

Tobias, Paul A. and David C. Trindade. *Applied Reliability*. 3 ed. Boca Raton, Fla.: CRC Press/Chapman & Hall, 2012.

Veers, P.S. "Statistical Considerations in Fatigue." In *Fatigue and Fracture*, 19, 295-302: ASM International, 1996.

Velay, V. Bernhart G. Delagnes D. Penazzi L. "A Continuum Damage Model Applied to High-Temperature Fatigue Lifetime Prediction of a Martensitic Tool Steel." *Fatigue and Fracture of Engineering Materials and Structures* 28, no. 11 (2005): 1009-1023.

APPENDIX A. SPECIMEN DRAWING AND MANUFACTURING METHOD

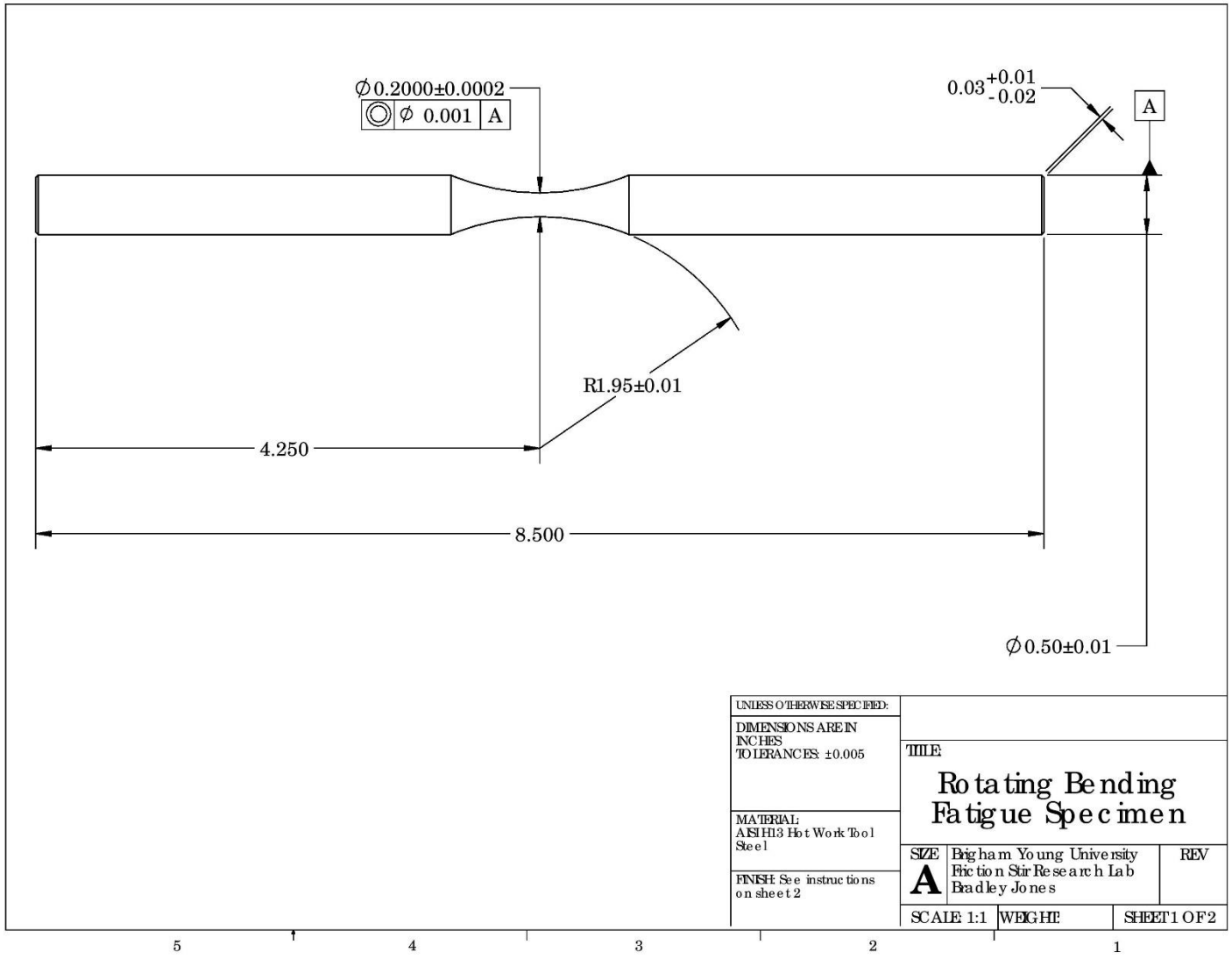

Figure A-1: Specimen Drawing (Image not to scale.)

Gage section machining instructions	
1	In the final stages of machining the gage section, remove material in small amounts until 0.005 in. of excess material remains.
2	Heat treat specimen (see Heat Treatment Instructions table).
3	Remove the next 0.004 in. of gage diameter by cylindrical grinding at a rate of no more than 0.0002 in/pass.
4	Remove the final 0.001 in. by polishing longitudinally to impart a maximum surface roughness of 8-µin. Ra, in the longitudinal direction. Gage section should be free of nicks, dents, scratches, and circumferential tool marks. Do not buff.

Heat Treatment Instructions	
1	Wrap specimens in stainless steel foil and place in oven at 1015C for 1 hour.
2	Remove tools and allow to air cool.
3	Temper tools for 1 hour in oven at 600C.
4	Turn off furnace and allow to cool with parts inside.

UNLESS OTHERWISE SPECIFIED:
DIMENSIONS ARE IN INCHES
TOLERANCES: ±0.005
MATERIAL:
AISI H13 Hot Work Tool Steel
FINISH: See instructions on sheet 2

TITLE:
Rotating Bending Fatigue Specimen

SIZE A | Brigham Young University, Friction Stir Research Lab, Bradley Jones | REV

SCALE: 1:1 | SHEET 2 OF 2

5 4 3 2 1

Figure A-2: Specimen manufacturing and heat treat process.